Organic Process Research & Development

Article

pubs.acs.org/OPRD

Establishment of a Continuous Sonocrystallization Process for Lactose in an Oscillatory Baffled Crystallizer

Humera Siddique, Cameron J. Brown, Ian Houson, and Alastair J. Florence*

EPSRC Centre for Innovative Manufacturing in Continuous Manufacturing and Crystallization, Technology Innovation Centre, University of Strathclyde, Glasgow, G1 1RD, United Kingdom

Supporting Information

ABSTRACT: Crystallization at production scale (>10 kg) is typically a poorly understood unit operation with limited application of first-principles understanding of crystallization to routine design, optimization, and control. In this study, a systematic approach has been established to transfer an existing batch process enabling the implementation of a continuous process in an oscillatory baffled crystallizer (OBC) using ultrasound. Process analytical technology (PAT) was used to understand and monitor the process. Kinetic and thermodynamic parameters have been investigated for lactose sonocrystallization using focused beam reflectance measurement (FBRM) (Mettler Toledo) and mid-infrared spectroscopy (mid-IR) (ABB) in a multiorifice batch oscillatory baffled crystallizer (Batch-OBC). This platform provides an ideal mimic of the mixing, hydrodynamics and operating conditions of the continuous oscillatory flow crystallizer (COBC) while requiring only limited material. Full characterization of the hydrodynamics of the COBC was carried out to identify conditions that deliver plug-flow behavior with residence times of 1−5 h. The results show that continuous crystallization offers significant advantages in terms of process outcomes and operability, including particle size distribution (mean particle size <1500 μm) of alpha lactose monohydrate (LMH), as well as reduced cycle time (4 h compared to the 13−20 h in a batch process). Continuous sonocrystallization was performed for the first time at a throughput of 356 g·h^{-1} for 12−16 h. During the run at near plug flow, with supersaturation and controlled nucleation using sonication, no issues with fouling or agglomeration were observed. This approach has demonstrated the capability to provide close control of particle attributes at an industrially relevant scale.

1. INTRODUCTION

A recent review of the literature has revealed an increasing number of patents and published applications demonstrating the increased intensity of activities in process engineering for continuous manufacturing of chemicals.[1] The benefits, often declared in continuous processing, include better product yields and quality; use of lower amount of solvent and other materials; less extreme operating conditions; more efficient consistent mixing; better control over process parameters; improved safety, improved purity profiles, and ease of scale-up.

In a manufacturing process, downstream processing stages can be a bottleneck to making a quality product in an economic, safe, and profitable way, as the components and processes involved are often time-consuming, inefficient, and poorly understood.

Crystallization is one of the most important downstream processes in determining the purity, form, shape, size, and size distribution of the final particles and is governed by complex interacting variables—a simultaneous heat and mass transfer process with a strong dependence on fluid and particle mechanics. A number of continuous reactor designs have been described and have the potential to deliver crystallization. These includes mixed suspension mixed product removal (MSMPR), continuous stirred tank reactor (CSTR) cascade systems, plug-flow reactors (PFRs), and oscillatory baffled crystallizers (OBC).[2−4]

A batch OBC has been investigated for a number of reactions,[2−7] but its use for crystallization has not received immediate attention.[2−7] The basic design and operating principle of OBC has been described elsewhere.[4,5] The basic design comprises a tubular network containing periodically spaced orifice baffles superimposed with oscillatory motion of a fluid. Oscillatory flow mixing has been developed and investigated as a process intensification technology to achieve efficient and controlled mixing in tubular crystallizers. Unlike conventional tubular crystallizers in which the mixing is caused by the turbulent net flow, the mixing achieved in an OBC is mainly obtained by fluid oscillations and thereby the residence time distribution within the device can be adjusted by the oscillatory conditions and net flow rate allowing longer residence times in short reactors and hence is more suitable for slower processes like crystallization.[7−12] Previous studies have shown that processing in an OBC resulted a greater regularity of crystal shape with fewer defects and better control over the crystallization process. A recent review provides a detailed description of OBCs for crystallization as well as summarizing the relevant literature.[63] These are attributed to the uniform mixing when compared to a batch stirred tank system.[3] Batch to continuous translation of crystallization processes can be achieved by maintaining same geometric ratios in continuous as in batch and ensuring similar values for oscillatory and net flow Reynolds number.[4]

In addition to the recent advances in developing continuous crystallization systems, use of process analytical technologies

Special Issue: Polymorphism & Crystallisation 2015

Received: April 17, 2015

DOI: 10.1021/acs.oprd.5b00127
Org. Process Res. Dev. XXXX, XXX, XXX−XXX

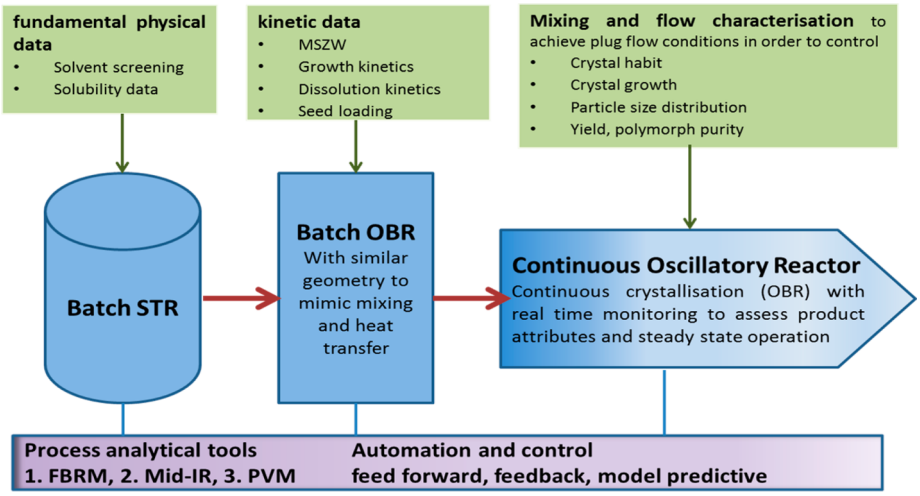

Figure 1. Sequence of steps to transfer from batch to continuous crystallization process.

(PAT) for real time monitoring of crystallization process is also progressing well.[13−15] For a crystallization process, it is important to know in real-time the stories of particle size distribution, crystal form, and the solution-phase concentration of active ingredient. With recent advances in technology, more online analytical tools have become available for these measurements.[13] Among these FBRM, particle vision measurement (PVM), Raman, ultraviolet (UV), and mid-IR spectroscopy are most commonly used analytical tools. These PAT help in relating OBC process conditions to the crystallization process and then to product attributes.

Lactose is a disaccharide of glucose and galactose with two isomeric forms, α and β, that interconvert by mutarotation and exist at equilibrium in solution.[16] When a lactose solution in water is supersaturated at moderate temperatures (below 95 °C), α lactose monohydrate (ALM) crystals will be obtained since the α form is less soluble and crystallization will continue so long as α-lactose in solution can be replenished fast enough by mutarotation.[16] Lactose cooling crystallization in batch under constant stirring from aqueous lactose solutions of different concentration results in varied crystal size, shape, and surface texture.[17−21] Induction times as long as 3−10 h with crystallization growth times ranging from 8−20 h are required to reach D90 of 85−100 μm. The yield varied from 45 to 60% with the lactose concentration from 44% to 53% (w/w). Further, these particles exhibited a wide particle size distribution (PSD) (particle span 3−4), resulting in a relatively small fraction of crystals in the desired size range.[17−21] In recent years sonocrystallization of lactose has been investigated to optimize crystallization time and particle size distribution.[22−29] Additionally, the implementation of sonocrystallization to OBC has already been achieved.[62]

A notable challenge in lactose crystallization is the long induction times. To overcome this problem seeding methodologies are adopted. Lactose sonocrystallization has shown rapid nuclei induction and crystal growth.[22,23] When ultrasound propagates through a liquid medium, its power is not only a driving force for mass transfer but also initiates an important phenomenon known as cavitation. When a cavitational bubble implodes, a localized hot spot is formed with a high temperature and pressure releasing a powerful shock wave. This cavitation generates high local supersaturation leading to spontaneous nucleation in otherwise unsaturated liquid. The acoustic streaming, microstreaming, and highly localized temperature and pressure within the fluid causes spontaneous induction of primary nucleation, reduction of crystal size, inhibition of agglomeration, and manipulation of crystal size distribution.[30−34] Sonication can promote fines in batch processes, so sonication should only be used for nucleation, and then production of larger crystals can be achieved by growth of those seed crystals.

This work sets out to develop a rational approach (Figure 1) (direct control) based on crystallization fundamentals to offer a continuous sonocrystallization process for ALM in a COBC (Rattlesnake from Cambridge Reactor Design). A sequence of steps is followed to acquire the relevant process parameters to enable the transfer from a batch to continuous process (Figure 1). The initial focus is on control of particle size with no fouling or blockage with direct control method and demonstration of the feasibility of continuous crystallization process for ALM and use of sonication for seed generation to control particle size distribution while maintaining a good yield.

2. MATERIALS AND METHODS

2.1. Materials. ALM and sodium benzoate (tracer material) were purchased from Sigma-Aldrich, UK.

2.2. Methods. *2.2.1. Crystallization Setup. 2.2.1.1. Batch crystallizer (Solubility Study, Thermodynamics).* Mettler Toledo "Optimax-1001" was used to determine the solubility profile and metastable zone width of ALM. The Optimax-1001 platform is a stirred tank crystallizer (STC) with a working volume of 1 L and a 45° pitched four-blade impeller. Ports are available in the STC to introduce process analytical tools such as FBRM, mid-IR, PVM, and thermocouples. Mid IR was used in the STC to measure the solubility of lactose at different temperatures.

2.2.1.2. Batch Oscillatory Baffle Crystallizer (Optimization of Cooling Profile, MSZW). The batch OBC used here consists of a glass jacketed cylindrical reactor, having a length of 500 mm and an internal diameter of 69 mm (Figure 2). The module contains 23 baffles, constructed from stainless steel with a FEP (fluorinated ethylene propylene) nonstick coating. The baffles are positioned 18 mm from one another with the openings in adjacent baffles aligned. Each baffle comprises 33 circular openings of 6 mm in diameter. Temperature control within the reactor is provided through a water filled jacket

DOI: 10.1021/acs.oprd.5b00127
Org. Process Res. Dev. XXXX, XXX, XXX−XXX

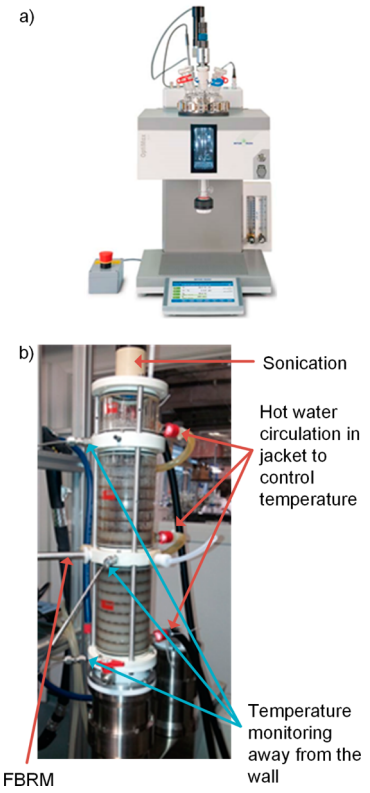

Figure 2. (a) Optimax (STC) and (b) batch OBR with FBRM and sonication equipment.

connected to a heater/chiller. The temperature is monitored at three different points: the top, middle, and bottom. Oscillatory mixing is provided by pistons operated using a hydraulic actuator. Lactose solution was introduced into the batch OBC from the top of the reactor. Cooling crystallization was performed using defined cooling profile. At the end of each crystallization, crystals were filtered using a vacuum filter and washed with pure ethanol. The crystals were allowed to dry at 40 °C in an oven for 24 h. After drying, a small amount of sample was taken from the batch for characterization.

2.2.1.3. Continuous Oscillatory Baffle Crystallizer (Rattlesnake from Cambridge Reactor Design). The COBC consists of four jacketed modules and has been described elsewhere.[35] The crystallizer is illustrated diagrammatically in Figure 3. Each module is cylindrical, constructed from polished stainless steel, having a length of 740 mm and an internal diameter of 69 mm. Each module has an internal baffle/obstruction design as described in Section 2.2.1.2. Temperature control within a module is provided through a double water filled jacket: a primary jacket arranged with liquid flow in a cocurrent configuration, within which a secondary coil is positioned with liquid flow in a counter-current configuration.[35] This shell and tube jacketed design provide a smooth temperature control, which is the most important parameter in cooling crystallization.

Temperature monitoring is possible at the junctions at the end of the modules allowing six monitoring points. Based on the temperature readouts, the operation of the water filled jacket on each module can be adapted to mimic a desired cooling profile. Oscillatory mixing is provided using the same mechanism as the batch platform. Both the frequency and the stroke of the piston can be varied on demand to achieve optimum mixing conditions and solid suspension.

The crystallization setup also includes means for initiating crystallization (Sonicator 4000, Misonix). The ultrasonic device can be located at any position at the ends of the module and can be operated in pulsed or continuous mode. The solution weight and the position of the probe inside the solution were kept constant for all experiments. The device works at a constant frequency of 20 kHz and allows the amplitude to change from 0 to 100%, delivering a power range between 10 and 70 W. Ultrasonic energy (Q) dissipated to the solution was calculated using a calorimetric method according to eq 1:

$$Q = (m_{\text{water}} C_{p,\text{water}} + m_{\text{lactose}} C_{p,\text{lactose}})(T_f - T_i) \quad (1)$$

where m is the weight of solution, C_p is the heat capacity, and T_f and T_i are the final and initial solution temperatures.[52] Heat capacities of lactose and water are 0.45 and 4.181 kJ·kg^{-1}·K^{-1} respectively. Power and energy density were expressed as W·g^{-1}.

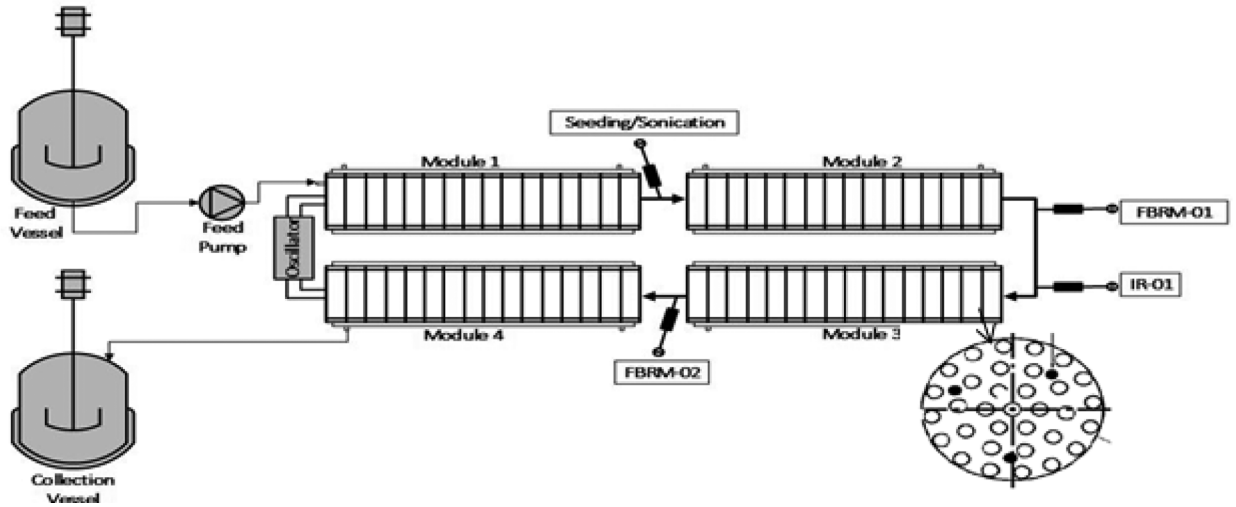

Figure 3. Schematic of continuous oscillatory baffle reactor (module details are taken from ref 35). The inset illustrates the baffle multiorifice design in plan view.

DOI: 10.1021/acs.oprd.5b00127
Org. Process Res. Dev. XXXX, XXX, XXX−XXX

2.2.2. Residence Time Distribution Characterization. To investigate the effect of oscillatory flow conditions on the mixing behavior in continuous crystallization, the residence time distribution was determined under different oscillatory conditions. The nature of oscillatory flow has been characterized quantitatively and qualitatively in previous studies.[7−12,42−48] Oscillatory flows are characterized by three dimensionless numbers, the oscillatory Reynolds number (eq 2), the velocity ratio (eq 3), and the Strouhal number (eq 4), defined as,

$$\mathrm{Re_o} = \frac{2\pi f \chi_o \rho d}{\mu} \tag{2}$$

$$\psi = \frac{\mathrm{Re_o}}{\mathrm{Re_n}} \tag{3}$$

$$\mathrm{St} = \frac{d}{4\pi\chi_o} \tag{4}$$

where $\mathrm{Re_o}$ is the oscillatory Reynold number, f is the frequency of oscillation (Hz), χ_0 is the amplitude of oscillation (m), ρ is the density of material (kg·m^{-3}), d is the column diameter (m), and μ is fluid viscosity (kg·m^{-1}·s^{-1}).

The axial dispersion coefficient D [eq 5; $D = E/uL$, where E is the axial dispersion number, u is the mean axial velocity (m·s^{-1}), and L is the length of reactor (m)] is used to describe the characteristics of mixing in continuous reactors.[36] It is a measure of the degree of deviation in flow from the true plug flow scenario: in theory it should be zero for truly plug flow behavior. The equation governing D in a continuous system is

$$\frac{dc}{dt} = D\frac{d^2c}{dx^2} - U\frac{dc}{dx} \tag{5}$$

where c is dimensionless concentration, t is dimensionless time, and x is dimensionless length. The dispersion model (eq 5), where the reactor is seen as a continuous path, is used to study RTD in oscillatory baffled flow systems. This model is applied on a continuous reactor when Bodenstein number is the range of 1−100.[2,36−41]

Most of the previous RTD studies[41] were performed by standard imperfect pulse injection techniques in which the concentration time profile at the two points of the system was measured and an axial dispersion model was applied following statistical analysis of data.[10]

Twelve milliliters of 20 g·L^{-1} sodium benzoate tracer was injected "instantaneously" above the feed position (Figure 4). A

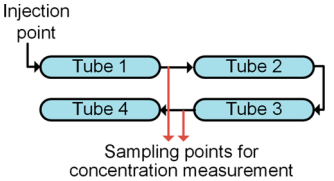

Figure 4. Injection and sampling points in rattlesnakes for RTD study.

UV transflectance probe positioned in situ at the end of the first and third straight of COBC is used to record absorbance against time as the tracer elutes. The λ_{max} for sodium benzoate in water was determined at 226 nm. Different concentrations of sodium benzoate were tested to establish the calibration for the absorbance to concentration conversion. The limit of detection for sodium benzoate was determined as 2.501 × 10^{-6} g·L^{-1} (signal: noise, 3:1). Finally, experimental concentration−time data was used to determine deviation from plug flow (D/uL). Operating conditions are summarized in Table 1.

2.2.3. Particle Size Analysis. Particle size was measured by a laser diffractometer, Mastersizer 3000 Ver.2.00 (Malvern Instruments, Malvern, UK). Analysis was done in triplicate, and mean results are presented as D10, D50, and D90. Ethanol was used as a dispersant, and obscuration was not less than 10% for each measurement. Data analysis was carried out using Malvern Software Version 5.2.

2.2.4. Chord Length Distribution from FBRM. The operating principle of FBRM has been described elsewhere.[15] All FBRM measurements were carried out using the Mettler Toledo G400-FBRM system.

2.2.5. Infrared Spectroscopy (IR). The mid-IR is an in-line based analytical technique in which information can be obtained via a probe about solution concentration, even in the presence of particles. The analysis is based on the mid-IR region (650−2000 cm^{-1}). In general the main condition is that a distinctive peak for the solute is present and can be separated from the chosen solvent. An ABB mid-IR MBX3000 system with the 12 mm diameter probe was used for this study.

2.2.6. Differential Scanning Calorimetry (DSC). DSC studies were carried out using NETZSCH DSC STA 449C instrument equipped with an intracooler (CC 200). Indium and zinc standards were used to calibrate the DSC temperature and enthalpy scale. The samples were pierced in aluminum crucibles and heated at a constant rate of 10 °C·min^{-1} over a temperature range of 25−250 °C. An inert atmosphere was maintained by purging helium gas at flow rate of 70 mL·min^{-1}.

2.2.7. X-ray Powder Diffraction Analysis (XRPD). The XRPD patterns were recorded on X-ray diffractometer. For sample fingerprinting, 10−50 mg of sample was placed on a 28 well plate supported on a polyimide (Kapton, 7.5 μm thickness) film. Data were collected on a Bruker AXS D8-Advance transmission diffractometer equipped with θ/θ geometry, primary monochromatic radiation (Cu Kα_1, λ = 1.54056 Å), a Vantec 1-D position sensitive detector (PSD), and an automated multiposition x−y sample stage. Data were collected in the range 4−35° 2θ with a 0.015° 2θ step size and 1 s step^{-1} count time. Samples were oscillated ±0.5 mm in the x−y plane at a speed of 0.3 mm·s^{-1} throughout data collection to maximize particle sampling and minimize preferred orientation effects.

2.2.8. Power Density Calculations in Crystallizers. The power density was calculated for MSZW comparison in an STR and batch OBR.

The equation used for power density calculation in Optimax (STC) is given below:

$$\epsilon_{\mathrm{STC}} = \frac{P_o \rho N_s^3 D_s^5}{V_L} \tag{6}$$

where P_o is the power number of impeller, ρ is the density of fluid (kg·m^{-3}), N is the rotational speed of impeller (s^{-1}), D_s is the diameter of impeller (m), and V_L is the volume of liquid (m^3). The power density for the batch OBC was calculated by using eq 7.

$$\epsilon_{\mathrm{OBC}} = \frac{2\rho N_b}{3\pi C_D^2}\left(\frac{1-S^2}{S^2}\right)\chi_o^3(2\pi f)^3 \tag{7}$$

DOI: 10.1021/acs.oprd.5b00127
Org. Process Res. Dev. XXXX, XXX, XXX−XXX

Table 1. Summary of the Oscillatory and Net Flow Conditions

flow rate (mL·min^{-1})	frequency (Hz)	amplitude (mm)	module length (mm)	T (min)	mean velocity (mm·s^{-1})	Re_n	Re_o	Ψ velocity ratio	St
130	8	1	740	23	19.2	223.2	585.1	2.6	1.0
130	8	2	740	23	19.2	223.2	1170.3	5.2	0.5
130	4	1	740	23	19.2	223.2	292.6	1.3	1.0
130	4	2	740	23	19.2	223.2	585.1	2.6	0.5
50	8	1	740	60	7.4	85.9	585.1	6.8	1.0
50	8	2	740	60	7.4	85.9	1170.3	13.6	0.5
50	4	1	740	60	7.4	85.9	292.6	3.4	1.0
50	4	2	740	60	7.4	85.9	585.1	6.8	0.5
130	8	1	2500	69	19.2	223.2	585.1	2.6	1.0
130	8	2	2500	69	19.2	223.2	1170.3	5.2	0.5
130	4	1	2500	69	19.2	223.2	292.6	1.3	1.0
130	4	2	2500	69	19.2	223.2	585.1	2.6	0.5
50	8	1	2500	180	7.4	85.9	585.1	6.8	1.0
50	8	2	2500	180	7.4	85.9	1170.3	13.6	0.5
50	4	1	2500	180	7.4	85.9	292.6	3.4	1.0
50	4	2	2500	180	7.4	85.9	585.1	6.8	0.5
130	2	1	740	23	19.2	223.2	146.3	0.7	1.0
130	2	1	2500	69	19.2	223.2	146.3	0.7	1.0

where f is frequency of oscillation (Hz), X_o is the center to peak amplitude of oscillation (m), S is the ratio of effective baffle area to tube area, C_D is discharge coefficient, and N_b is the number of baffles per unit length.

In calculating the values of Re_n, Re_o, and St, each term was redefined to account for the multi orifice geometry: the characteristic dimension d (formerly the crystallizer diameter) was replaced by de (equivalent diameter of a notional tube surrounding each orifice), which was the diameter equivalent to the total baffle area divided by the number of orifices.[12,41] T is the residence time calculated based on volume and volumetric flow rate of each module

3. RESULTS AND DISCUSSION

3.1. Solubility and Metastable Zone Width (MSZW) Investigation. Initial dissolution of ALM occurs rapidly upon addition of solid to water. Subsequently, as mutarotation occurs and conversion from alpha lactose to beta lactose proceeds, then more alpha lactose dissolves until the equilibrium ratio of isomers is reached.[49] The rate-determining step of dissolution is the mutarotation of isomers.[50] Hence the final solubility of lactose can be determined by adding excess alpha lactose monohydrate to water and agitating it, at constant temperature for long enough to establish the mutarotation and solubility equilibria. To investigate the solubility of alpha lactose monohydrate an in situ Mid IR probe (reactIR, Mettler Toledo) was used. A 1 L feed solution was prepared by adding 60 wt % of lactose and stirred at 200 rpm. A program was established to obtain the solubility curve based on the equilibrium dissolution point of ALM solid in contact with aqueous solution. The solution was heated from 0 to 10 °C at a rate of 0.1 °C·min^{-1} and then held at this temperature for 8 h until a constant peak area from the IR probe indicated and the mutarotation and solubility equilibrium had been reached. This procedure was performed continuously at 10 °C intervals between 10 and 80 °C (Figure 5). After the preprocessing of spectral data (second order derivative), the equilibrium concentration points were plotted to obtain the temperature-dependent solubility curve (Figure 5). Concentration calibration on data from Mid-IR was performed using PharmaMV software (Perceptive Engineering).[54]

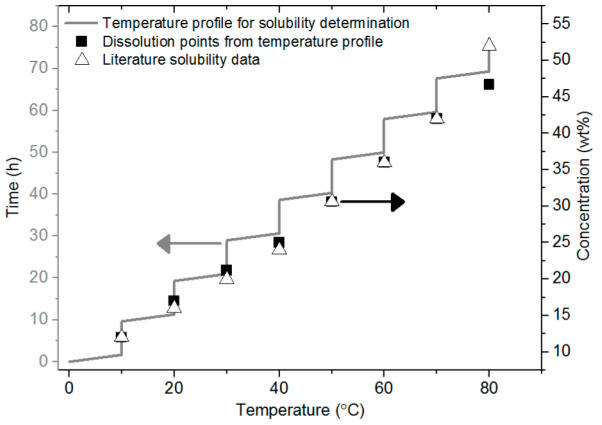

Figure 5. Comparison of solubility curve from the literature with experimentally derived solubility curve in the STC and programmed temperature profile for determination of the temperature-dependent equilibrium solubility points.

The MSZW was investigated using IR and FBRM to detect concentration and nucleation, respectively. In the STC, a 1 L solution of 47% (w/w) lactose was introduced. The pitched blade agitator speed was set at 900 rpm, and the solution was cooled at a rate of 0.18 °C·min^{-1}. This experiment was also performed at 500 and 200 rpm. Nucleation was detected by the particle count on the FBRM and concentration drop. A similar procedure was adopted to get the MSZW in the batch OBC. 1.8 L of feed solution was introduced into the batch OBC and cooled at 0.18 °C·min^{-1} using 4 Hz and 1 mm oscillatory conditions. The MSZW is narrower in the STC compared to the batch OBC operated at 900 rpm as shown in Figure 6. It has been reported that the volume averaged shear rate in OBCs is generally of order 10−20 s^{-1}, which is significantly lower than that in stirred tank crystallizers (STC), which are typically 100 s^{-1} or greater.[51] Power density[51] calculations were carried out for both reactors showing the power density to be 50 times lower in the batch OBC as compared to STC for the same MSZW (Table 2). Abbott et al.[55] has made a comparison of

DOI: 10.1021/acs.oprd.5b00127
Org. Process Res. Dev. XXXX, XXX, XXX−XXX

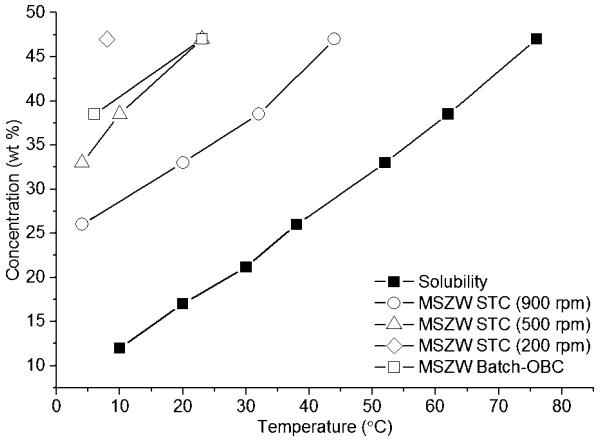

Figure 6. MSZW in STC at 900 rpm, 500 rpm, 200 rpm, and batch OBC operated at 4 Hz frequency and 1 mm amplitude. Table 2 summarizes the power density values under each condition.

Table 2. Mixing Conditions and Power Density for Optimax (STC) and Batch OBC

system	mixing (rpm/Re_o)	power density ($W \cdot m^{-2}$)
STC	200	54
STC	500	841.3
STC	900	3447
batch OBC	300	10

power consumption in an OBR vs STR for enzymatic saccharification of alpha cellulose. According to their study, 2.36 $W \cdot m^{-3}$ power input was sufficient to produce maximum conversion in the OBR which was 12% higher after 24 h and 25% higher after 6 h than the STR (250 $W \cdot m^{-3}$ required for equivalent conversion). They concluded that efficient mixing performance in an OBR at very low power density is responsible for higher conversion. Unlike STRs that rely on stirring mechanisms for mixing, the OBR uses oscillations to produce vortices. These form periodically along the entire length of the reactor, effectively causing each interbaffle zone to act as a CSTR; the entire reactor therefore consists of a large finite number of CSTRs connected in series.[59]

3.2. Mixing and Flow Characterization of COBC. The aim of this study was to produce a design space of operating parameters to ensure plug flow conditions are achieved in the COBC during operation. The axial dispersion coefficient was analyzed for different oscillatory and net flow conditions (amplitude, frequency, and flow rate). These flow conditions were established based on accepted ranges of Re_o, St, Re_n, and Ψ for traditional continuous oscillatory baffled crystallizers.[7−12] In a continuous crystallizer, the mean residence time can be used as a basis to determine Re_n. When Re_n is known, the frequency and amplitude should be chosen such that Re_o satisfies the velocity ratio, in the range 2−10 (range selected based on previous RTD studies in oscillatory flow crystallizers[8,10]). Another important factor is terminal velocity calculations for particle suspension at the above-mentioned flow conditions. Solid loading was reduced for lactose crystallization to 33 wt % to maintain particle suspension in the COBC under these design conditions.

Experimental RTD response is presented in Figures 7 and 8. For each value of flow rate investigated, the RTD response can be seen to be dependent on both frequency and amplitude of oscillation. There is an optimum range of frequency and amplitude at which the system displays a minimum axial dispersion coefficient which is the desired state for near plug flow operation.

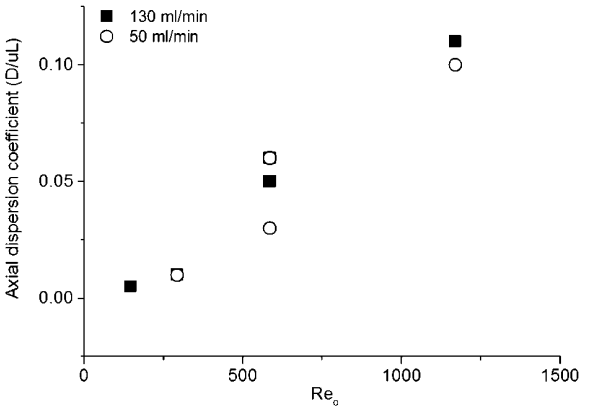

Figure 7. Relationship between axial dispersion coefficient and oscillatory Reynolds number at experimental net flow conditions.

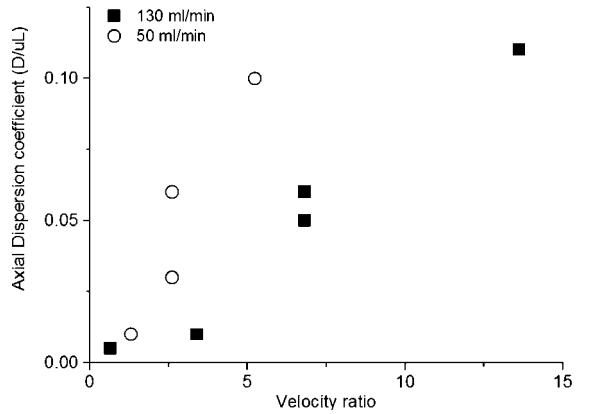

Figure 8. Relationship between axial dispersion coefficient and velocity ratio at experimental net flow conditions.

Based on the results above, there is an effective minimum value of axial dispersion in the range of $100 \leq Re_o \leq 400$, which is an acceptable limit (axial dispersion below 0.02) for plug flow in a reactor. These results are consistent with the experimental literature observations for sharp edge baffled systems.[9,12] At these Re_o values the vortices formed as a result of oscillations are powerful enough to give effective radial mixing. These results also indicate that the axial dispersion coefficient decreases with increasing Re_n, which indicates that as expected net flow rate improves the overall RTD performance. It is clear from Figure 8 that, with velocity ratio 1−5, a reasonable plug flow response is achievable.

3.3. Optimisation of Cooling Profile and Sonication. The effect of sonication energy density and residence time on particle size and yield was investigated for 33 wt % lactose feed solution. To achieve minimum axial dispersion the oscillatory conditions were fixed at a frequency of 4 Hz and 1 mm amplitude. A cooling profile for crystallization process was established by applying direct control (model predictive control)[55] on supersaturation using the PharmMV control system from Perceptive Engineering.[54] The methodology for sonocrystallization in batch-OBC and COBC is presented in Figure 9. Sonication was introduced at a fixed supersaturation of 1.2. Results of sonocrystallization studies from batch

DOI: 10.1021/acs.oprd.5b00127
Org. Process Res. Dev. XXXX, XXX, XXX−XXX

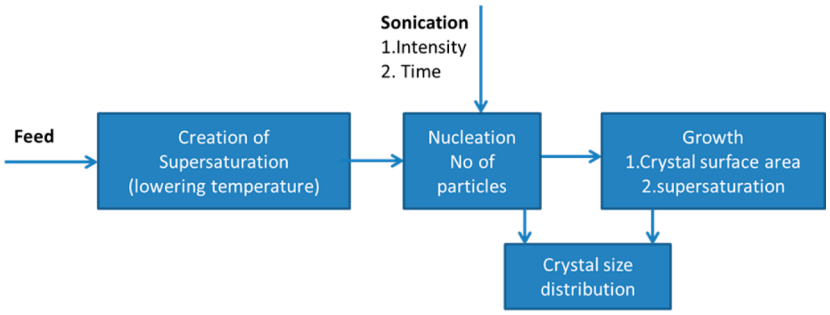

Figure 9. A simple information flow diagram for sonocrystallization of lactose in batch OBC and COBC.

Table 3. Batch Lactose Crystallization with Varying Sonication Power and Residence Time with Kinetic Parameters Estimated by the Previously Described Population Balance Model

residence time (h)	sonication power ($W \cdot g^{-1}$)	yield %	mean particle size (μm)	$\ln(k_b)$	b	$-\ln(k_g)$	g
2.5	0.10	17.4 ± 0.7	1010 ± 10	17.627	2.137	5.425	3.765
2.5	0.15	25.1 ± 0.5	970 ± 7	23.219	5.112	7.641	2.195
4.0	0.10	19.7 ± 0.8	1530 ± 9	22.205	5.960	5.728	3.476
4.0	0.15	28.3 ± 0.7	1150 ± 6	28.049	8.679	6.597	2.922

experiments are presented in Table 3. Nalajala et al.[48] investigated the physical mechanism of sonocrystallization for a KCl−methanol−water system and reported that the shock waves created by ultrasound affected nucleation, while micro turbulence (microconvection) governed the growth rate.

One major benefit of sononucleation is the reproducibility of the size and number of nuclei; the use of ultrasound to generate nuclei in a controlled and reproducible way provides therefore a well-defined starting point for the crystallization process through consistent surface area available for growth.[53] This enables control of the crystal growth via supersaturation and residence time in the crystallizer. It has been reported in the literature that crystal size distribution can be tailored by optimizing sonication intensity.[53] From batch work it has been shown that a short burst of ultrasound generates small number of nuclei allow their growth to a larger crystal size. However, continuous (or perhaps a single long burst) sonication can produce a large number of small crystals. In this study a short burst of sonication was introduced in lactose solution at a supersaturation of 1.2, and then cooling crystallization was performed to grow the generated nuclei from sonication as explained in Figure 9. Table 3 summarizes the sonication power delivered in batch system and kinetic parameters estimated using population balance model.

When only a one-dimensional characteristic size is considered, the jth moment can be defined as

$$\mu_j = \int_0^\infty L^j f_n(L, t)\mathrm{d}L \tag{8}$$

where $f_n(L,t)$ is the crystal size distribution, t is the time, and L is the characteristic crystal size. Therefore, a complete model of the crystallization process can be described by considering the first five moment equations and the mass balance equation[56] as

$$\begin{bmatrix} \mathrm{d}\mu_0/\mathrm{d}t \\ \mathrm{d}\mu_1/\mathrm{d}t \\ \mathrm{d}\mu_2/\mathrm{d}t \\ \mathrm{d}\mu_3/\mathrm{d}t \\ \mathrm{d}\mu_4/\mathrm{d}t \\ \mathrm{d}C/\mathrm{d}t \end{bmatrix} = \begin{bmatrix} B \\ G\mu_0 + BL_0 \\ 2G\mu_1 + BL_0^2 \\ 3G\mu_2 + BL_0^3 \\ 4G\mu_2 + BL_0^4 \\ -\rho_c k_v(3G\mu_2 + BL_0^3) \end{bmatrix}$$

where C is the solution concentration (g/mL water), L_0 is the crystal size at nucleation, ρ_c the crystal density (1.545 g/mL for lactose),[57] k_v the volume shape factor (0.524),[57] and B and G are the primary nucleation and size independent growth rates, respectively, which are described by the power law expressions:

$$B = k_b \Delta C^b \tag{9}$$

$$G = k_g \Delta C^g \tag{10}$$

The calculations of the fourth and third moments allow for the determination of the volume mean size (L_{43}) of the crystal size distribution:

$$L_{43} = \frac{\mu_4}{\mu_3} \tag{11}$$

In addition the solubility of lactose (g/mL water) as a function of temperature, T (in °C), is defined by

$$C = 0.1098e^{0.0276T} \tag{12}$$

For unseeded systems, the initial conditions for the moments and mass balance are defined as $\mu_i(0) = 0$ (i = 0, 1, 2, 3, 4, 5) and $C(0) = C_i = C(@50\ °C)$. Furthermore, the size of the nuclei is considered negligible ($L_0 = 0$).[58]

Solutions of the system of differentials were obtained by utilizing a Runge−Kutta numerical integration from the time at which ultrasound was activated to the end of the cooling profile. The kinetic parameters (k_b, b, k_g, and g) were estimated by performing a nonlinear optimization via a multiobjective genetic algorithm to minimize the root-mean-square deviation (RMSD) between the experimental measurements and model

DOI: 10.1021/acs.oprd.5b00127
Org. Process Res. Dev. XXXX, XXX, XXX−XXX

predictions. The values of L_{43} and C at the end of the cooling profile were chosen as the two objectives for the estimation:

$$\text{obj}_1 = \sqrt{(L_{43}^{\text{exp}} - L_{43}^{\text{pred}})^2_{@t,\text{end}}} \quad (13)$$

$$\text{obj}_2 = \sqrt{(C^{\text{exp}} - C^{\text{pred}})^2_{@t,\text{end}}} \quad (14)$$

Overall yield was low in all sonocrystallization experiments due to low sonication energy density applied. By varying residence time, a change in particle size distribution was observed in batch experiments (Table 3). It can be seen from Table 3 that, with an increase in sonication power, product yield was increased, and particle size was decreased as more nuclei were formed.

In all experiments, a bimodal particle size distribution was observed. Lactose has a very slow growth rate, and a large surface area is required to achieve good yield in the process over the residence times studied. Insufficient nuclei were generated by sonication to produce high yield, as sonication power was limited by the specific probe used. Therefore, the degree of supersaturation increased during the crystallization from the target of 1.2−1.4 as shown in Figure 10a. This higher supersaturation may be responsible for observed secondary nucleation and consequent fines in the product (Figure 10c). Attrition could be another reason for the appearance of smaller particles in the product. The particle size distribution and yield can be optimized by providing high power sonication energy with the help of multiple probes along the length of the reactor. The benefit of using multiple probes is to avoid extra heat generation which could be a problem with one high power ultrasound source and better control on sonication intensity. Another possible way to reduce fines is to control supersaturation with the help of a slow quadratic cooling profile and hence providing a longer residence time.

3.4. Continuous Lactose Crystallization in COBC. To maximize the yield, based on the batch work, a 4 h mean residence time was selected for continuous crystallization, using a feed flow rate of 50 mL·min^{-1}, frequency of oscillation 4 Hz, and amplitude of oscillation 1 mm. The scale up operation in the COBC was carried out by implementing the same conditions as identified from the batch OBC experiments described in section 3.2. Oscillatory conditions were selected based on residence time distribution study to achieve near plug flow in COBC (section 3.3). Sonication was introduced at the start of the second straight at a supersaturation of 1.2 to generate seeds (0.15 W·g^{-1}). FBRM and reactIR probes were placed at the end of second straight to monitor the state of the process.

At the start of the process, the COBC was filled with water, and the required temperature profile was achieved by controlling the cold and hot water flow in the jacket side of the crystallizer. Once the required temperature profile was achieved, the saturated feed solution was introduced in the crystallizer. The system was run for three residence times, and the product collected was analyzed using DSC and laser diffraction for particle size. The system attained steady state after one and a half residence times as shown in Figures 11 and 12. No signs of fouling or blockage were observed during the continuous trial. Images of the crystals produced in the COBC showed that the crystals were of the well-known tomahawk shape (Figure 13).

The product form was confirmed as ALM by DSC, TGA, and XRPD. Full data can be found in Supporting Information.

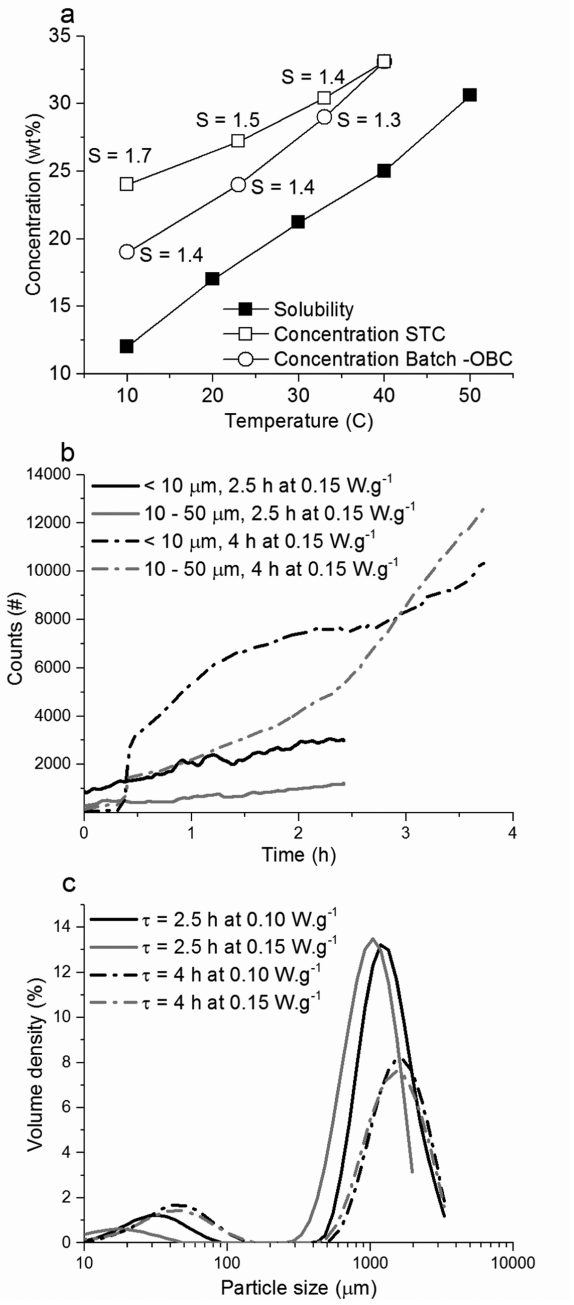

Figure 10. (a) Concentration profile for seeded lactose sonocrystallization in the STC and Batch-OBC (4 h, 0.15 W·g^{-1}) showing the different desupersaturation levels achieved. (b) FBRM data for lactose crystallization in batch OBC indicating secondary nucleation during the process due to elevated supersaturation after 2 h. (c) Particle size distribution for batch sonocrystallization in batch-OBC (Each set of conditions was repeated three times, and the coefficient of variation was less than 5%).

The crystals obtained from the COBC had similar bimodal particle size distribution (PSD) and morphology (Figure 14) as obtained from the batch OBC experiments with a mean particle size of 1530 μm. However, a wider particle span and slow particle growth was observed in the STC as compared to batch OBC and COBC. It has been reported previously that mass transfer coefficient is approximately 75% higher in the OBC as compared to the STC.[60] The yield was higher (38%) in the continuous trial compared to batch OBC (28.3%) which could

DOI: 10.1021/acs.oprd.5b00127
Org. Process Res. Dev. XXXX, XXX, XXX−XXX

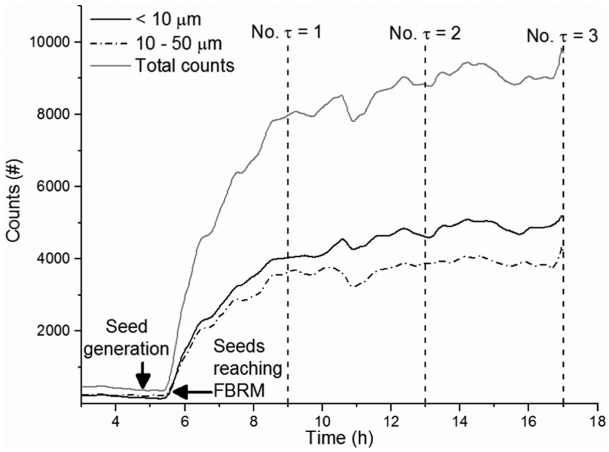

Figure 11. FBRM data showing steady state after one and half residence time during a 4 h cooling profile.

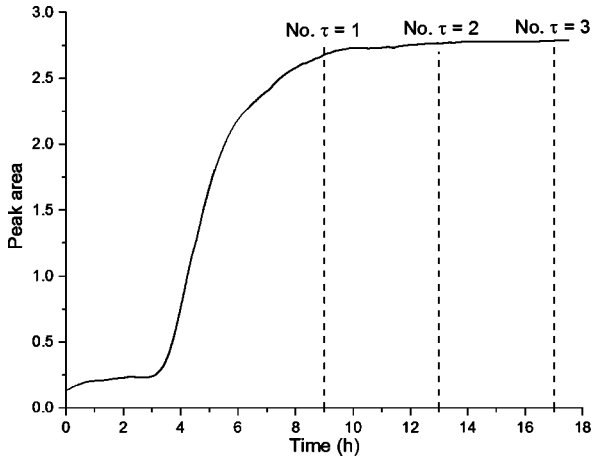

Figure 12. ReactIR data showing approximate steady state after two residence times in 4 h cooling profile.

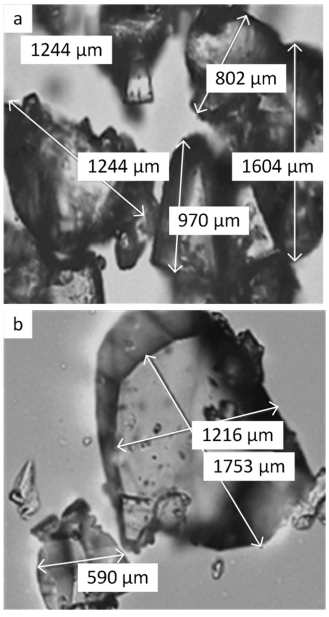

Figure 13. Images of crystals from continuous crystallization process (a) second residence time and (b) third residence time.

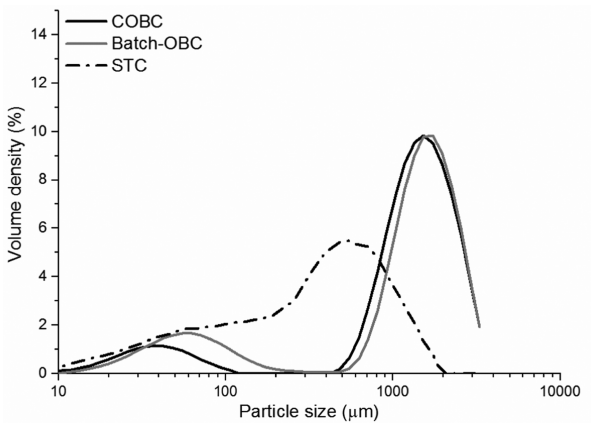

Figure 14. Particle size analysis of final product in three crystallizers.

be associated with more even distribution of shear rate, which on average leads to thinner liquid film (reduced boundary layer thickness).[61] The intensity of mixing is known to affect the mass transfer process in which solute leaves the solution and becomes part of the crystal. The high intensity of mixing enhances the mass transfer process, increasing the amount of solute incorporated into the solid phase. In case of continuous operation, net flow rate is an important factor increasing the overall mixing intensity consequently increasing the mass transfer. However, overall product attributes confirmed that the methodology established to move from batch to continuous COBC operation achieved the same product form with a higher yield. Further work is in progress to optimize the crystallization process to deliver improved control on product attributes, size, impurity rejection, and yield and will be reported in subsequent papers in this series.

4. CONCLUSION

A new systematic approach has been proven to develop a continuous sonocrystallization process using inline PAT and direct control approach. Thermodynamic and kinetic parameters were established for lactose crystallization using FBRM and mid-IR. Sonication was used to initiate nucleation, and the cycle time has been successfully reduced from 13 to 20 h in batch to 4 h in this COBC. The yield was relatively low compared with previous studies on batch lactose sonocrystallization due to the limitations of the maximum power generation from the sonicator used here generating insufficient seeds. As a result of not being able to generate enough nuclei secondary nucleation and fines, generation was observed at the end of the process which can be minimized by further improvements in providing multiple sonication generation units within the crystallizer and control of supersaturation through optimization of process. Narrower particle size distribution of crystals as compared to batch process with ability to vary D50 is achievable in continuous sonocrystallization process established in current work. With the ability to run COBC system for 1−5 h under near plug flow conditions, continuous sonocrystallization was successfully performed for the first time in COBC at a throughput of 356 $g \cdot h^{-1}$ with a consistent product quality and product attributes for 12 h. Further studies are under progress for optimization of lactose crystallization using process analytical tools and control models.

DOI: 10.1021/acs.oprd.5b00127
Org. Process Res. Dev. XXXX, XXX, XXX−XXX

■ ASSOCIATED CONTENT

Supporting Information

The Supporting Information is available free of charge on the ACS Publications website at DOI: 10.1021/acs.oprd.5b00127.

DSC and XRPD analysis of lactose feed stock and product (PDF)

■ AUTHOR INFORMATION

Corresponding Author

*E-mail: alastair.florence@strath.ac.uk.

Author Contributions

These authors contributed equally.

Funding

EPSRC funding was provided under grant reference: MOPPS: Made To Order Processing Plants 101334.

Notes

The authors declare no competing financial interest.

■ ACKNOWLEDGMENTS

The authors thank the EPSRC Centre for Continuous manufacturing and crystallization (www.cmac.ac.uk) for supporting this work. Authors would like to thank Technology Strategy board for funding. Authors would also like to thanks Metler Toledo, Perceptive Engineering and ABB for technical support.

■ ABBREVIATIONS

ALM	Alpha lactose monohydrate
Batch-OBC	Batch oscillatory baffled crystallizer
COBC	Continuous oscillatory flow crystallizer
CSTR	Continuous stirred tank reactor
DSC	Differential scanning calorimetry
FBRM	Focused beam reflectance measurement
FEP	Fluorinated ethylene propylene
MSMPR	Mixed suspension mixed product removal reactor
MSZW	Metastable zone width
Mid-IR	Mid infrared
PAT	Process analytical technologies
PFR	Plug flow reactor
PSD	Particle size distribution
PVM	Particle vision measurement
RTD	Residence time distribution
STC	Stirred tank crystallizer
XRPD	X-ray powder diffraction

Nomenclature

Re_o	Oscillatory Reynolds number
Re_n	Net flow Reynolds number
St	Strouhal number
χ_o	Centre to peak amplitude (mm)
d	Tube diameter (mm)
μ	Fluid viscosity ($kg{\cdot}m^{-1}{\cdot}s^{-1}$)
f	Frequency
ψ	Velocity ratio
t	Dimensionless time
E	Exit age distribution
D	Axial dispersion coefficient
u	Mean axial velocity
c	Dimensionless concentration
x	Dimensionless length
l	Length of reactor
ϵ	Power density
P_o	Power number for impeller
V_L	Volume of liquid
N_s	Rotational speed of impeller
D_s	Diameter of impeller
N_b	Number of baffles per unit length
C_d	Discharge coefficient
S	Ratio of orifice area to baffle area
C_p	Heat capacity
T_f	Final solution temperature
T_i	Initial solution temperature
m	Weight of solution
f_n (L,t)	Crystal size distribution
L	Characteristic crystal size
C	Solution concentration ($g.ml^{-1}$ water)
r_0	Crystal size at nucleation
ρ_c	Crystal density
k_v	Volume shape factor
B	Primary nucleation
G	Size independent growth rates

■ REFERENCES

(1) Hessel, V.; Knobloch, C.; Lowe, H. *Recent Patents Chem. Eng.* **2008**, *1*, 1−16.

(2) Mackley, M. R. *Chem. Eng. Res. Des.* **1991**, *69*, 197.

(3) Ni, X.; Mackley, M. R.; Harvey, A. P.; Stonestreet, P.; Baird, M. H. I.; Rao, N. V. R. *Chem. Eng. Res. Des.* **2003**, *81*, 373.

(4) Stonestreet, P.; Harvey, A. P. *Chem. Eng. Res. Des.* **2002**, *31*, 80.

(5) Abbott, M. S. R.; Harvey, A. P.; Perez, G. V.; Theodorou, M. K. *Interface Focus* **2013**, *3*, 20120036.

(6) Nogueira, X.; Taylor, B. J.; Gomez, H.; Colominas, I.; Mackley, M. R. *Comput. Chem. Eng.* **2013**, *49*, 1.

(7) Stonestreet, P.; Vander Veeken, P. M. J. *Trans IChemE* **1999**, *77*, 671.

(8) Dickens, A. W.; Mackley, M. R.; Williams, H. R. *Chem. Eng. Sci.* **1989**, *44*, 1471−1479.

(9) Neves-Saravia, R. M. D. C.; Maclay, M. R. *Proc. AIChE Jubilee research event* **1997**, *1*, 58.

(10) Howes, T.; Mackley, M. R. *Chem. Eng. Sci.* **1990**, *45*, 1349.

(11) Ni, X. W. J *J. Chem. Technol. Biotechnol.* **1995**, *64*, 165.

(12) Smith, K. R.; Mackley, M. R. *Cem. Eng. Res. Des* **2006**, *84*, 1001−1011.

(13) Barrett, P.; Glennon, B. *Trans IChemE* **2002**, *80*, 799−805.

(14) Kail, N.; Marquardt, W.; Briesen, H. *Ind. Eng. Chem. Res.* **2009**, *48*, 2936−2946.

(15) Preikschat, F. K.; Preikschat, E. U.S. Patent 4, 1989, *871*, 251.

(16) Raghavan, S. L.; Ristic, R. I.; Sheen, D. B.; Sherwood, J. N. *J. Pharm. Sci.* **2001**, *90*, 823−832.

(17) Raghavan, S. L.; Ristic, R. I.; Sheen, D. B.; Sherwood, J. N. *J. Phys. Chem. B* **2000**, *104*, 12256−12262.

(18) Thurlby, J. A.; Sitnai, O. *J. Food Sci.* **1976**, *41*, 43−47.

(19) Thurlby, J. A. *J. Food Sci.* **1976**, *41*, 38−42.

(20) Shi, Y.; Liang, B.; Hartel, R. W. *J. Food Sci.* **1990**, *55*, 817−820.

(21) Liang, B.; Shi, Y.; Hartel, R. W. *J. Food Sci.* **1991**, *56*, 848−854.

(22) Bund, R. K.; Pandit, A. B. *Chem. Eng. Process.* **2007**, *46* (9), 846−850.

(23) Bund, R. K.; Pandit, A. B. *Ultrason. Sonochem.* **2007**, *14* (2), 143−152.

(24) Arakelyan, V. S. *Acta Physica Hungarica* **1987**, *61*, 185−187.

(25) Arends, B. J. Blindt, R. A. Janssen, J. Patrick, M. United States Patent. US 6,630,185 B2, 2003.

(26) Chow, R.; Blindt, R.; Chivers, R.; Povey, M. *Ultrasonics* **2003**, *41*, 595−604.

(27) Dhumal, R. S.; Biradar, S. V.; Paradkar, A. R.; York, P. *Pharm. Res.* **2008**, *25* (12), 2835−2844.

(28) Ganzle, M. G.; Haase, G.; Jelen, P. *Int. Dairy J.* **2008**, *18*, 685−694.

DOI: 10.1021/acs.oprd.5b00127
Org. Process Res. Dev. XXXX, XXX, XXX−XXX

(29) Kougoulos, E.; Marziano, I.; Miller, P. R. *J. Cryst. Growth* **2010**, *312* (23), 3509−3520.
(30) Patel, S. R.; Murthy, Z. V. P. *Cryst. Res. Technol.* **2011**, *46* (3), 243−248.
(31) Patel, S. R.; Murthy, Z. V. P. *Sep. Purif. Rev.* **2012**, *41* (4), 251−266.
(32) Nii, S.; Takayanagi, S. *Ultrason. Sonochem.* **2014**, *21*, 1182−1186.
(33) Li, H.; Guo, Z.; Liu, Y. *Ultrason. Sonochem.* **2006**, *13*, 359−363.
(34) Renuka Devi, K.; Raja, A.; Srinivasan, K. *Ultrason. Sonochem.* **2015**, *24*, 107.
(35) Crystallisation process and apparatus, WO 2011/051728 A1.
(36) Levenspiel, O. *Chemical reaction engineering*, 3rd ed.; Wiley: New York, USA, 1999.
(37) Phan, A. N.; Harvey, A. P. *Chem. Eng. J.* **2012**, *180*, 229.
(38) Phan, A. N.; Harvey, A. P.; Lavender. *Chem. Eng. Process.* **2011**, *50*, 254.
(39) Phan, A. N.; Harvey, A. P. *Chem. Eng. J.* **2011**, *169*, 339.
(40) Phan, A. N.; Harvey, A. P. *Chem. Eng. J.* **2010**, *159*, 212.
(41) Smith, K. B. University of Cambridge, 1999.
(42) Zheng, M. Z.; Mackley, M. *Chem. Eng. Sci.* **2008**, *63*, 1788.
(43) Mackley, M. R.; Ni, X. *Chem. Eng. Sci.* **1991**, *46*, 3139.
(44) Mackley, M. R.; Ni, X. *Chem. Eng. Sci.* **1993**, *48*, 3293.
(45) Ni, X. W. *J. Chem. Technol. Biotechnol.* **1994**, *59*, 213.
(46) Mackley, M. R.; Stonesstreet, P.; Roberts, E. P. L.; Ni, X. *Chem. Eng. Res. Des.* **1996**, *74*, 541.
(47) Fitch, A. W.; Ni, X. *Chem. Eng. J.* **2003**, *92*, 243.
(48) Reis, N.; Vicente, A. A.; Teixeira, J. A.; Mackley, M. R. *Chem. Eng. Sci.* **2004**, *59*, 4967.
(49) Nalajala, V.; Moholkar, V. *Ultrason. Sonochem.* **2011**, *18*, 345−355.
(50) Roetman, K. *Voedings Middelen Technologie* **1972**, *3* (43), 230−239.
(51) hodges, G. E.; lowe, E. K.; Paterson, A. H. G. *Chem. Eng. J.* **1993**, *53*, B25−B33.
(52) Ni, X.; Mackley, M. R.; Harvey, A. P.; Stonestreet, P.; Baird, M. H. I.; Rama Rao, N. V. *Trans IChemE* **2003**, *81*, 373−383.
(53) Mason, T. J.; Lorimer, J. P.; Bates, D. M. *Ultrasonics* **1992**, *30*, 40−42.
(54) Gogate, P. R.; Pandit, A. B. *Food Eng. Series* **2011**, 467−493.
(55) Abbott, M. S. R. *Chem. Eng. Res. Des.* **2014**, *92*, 1969−1975.
(56) Randolph, A. D.; Larson, M. A. *Theory of particulate processes: analysis and techniques of continuous crystallization*; Academic Press, 1988.
(57) Amira, R.; Dominikus, N. *arXiv*: 1305.1043 [math.OC], **2013**.
(58) Nagy, Z. K.; et al. *Ind. Eng. Chem. Res.* **2008**, *47*, 1245−1252.
(59) Abbott, M. S. R.; Harvey, A. P.; Perez, G. V.; Theodorou, M. K. *Interface Focus* **2013**, *3*, 20−36.
(60) Oliveira, M. S. N.; Ni, X. *Chem. Eng. Sci.* **2001**, *56*, 6143−6148.
(61) Ni, X.; Gao, S. *Chem. Eng. Sci.* **1995**, *50* (13), 2127−2136.
(62) Ruecroft, G.; Burns, J. Patent No. WO 2010079350 A2, 2010.
(63) McGlone, T.; Briggs, N. E. B.; Clark, C. A.; Brown, C. J.; Sefcik, J.; Florence, A. J. *Org. Process Res. Dev.* **2015**, *19*, 1186.
(64) http://www.perceptiveapc.com/products/pharmamv/ (last accessed March 4, 2015).

DOI: 10.1021/acs.oprd.5b00127
Org. Process Res. Dev. XXXX, XXX, XXX−XXX